Preparation of the new heteronuclear α-diimine complexes $FeRu(CO)_6$(R-Pyca) and $Fe_2Ru(CO)_{10}$(R-Pyca) (R-Pyca = C_5H_4N-2-CH=NR); ^{13}C NMR study of the fluxional behaviour of the carbonyl ligands in $Fe_2Ru(CO)_{10}$(R-Pyca)

Marco J. A. Kraakman, Cornelis J. Elsevier, Jan-M. Ernsting, Kees Vrieze*

Laboratorium voor Anorganische Chemie, J. H. van't Hoff Instituut, Universiteit van Amsterdam, Nieuwe Achtergracht 166, 1018 WV Amsterdam (Netherlands)

and Kees Goubitz

Laboratorium voor Kristallografie, J. H. van't Hoff Instituut, Universiteit van Amsterdam, Nieuwe Achtergracht 166, 1018 WV Amsterdam (Netherlands)

(Received June 10, 1992)

Abstract

$Ru_2(CO)_4(L)_2$ (L = R-Pyca, R = ^{i}Pr (**1a**); R = ^{c}Hex (**1b**); R = ^{t}Bu (**1c**)) reacts with $Fe_2(CO)_9$ (**2**) at room temperature to give the new complexes $FeRu(CO)_6$(R-Pyca) (**3a–c**) and $Fe_2Ru(CO)_{10}$(R-Pyca) (**4a–c**). Although the reaction proceeds also for L = R-DAB, it is synthetically useful only for L = R-Pyca. The complexes **3a–c** can also be prepared by thermal conversion of **4a–c** at 70 °C in nearly quantitative yields. X-ray single crystal structures of the complexes **3a** and **4a** have been determined. Red crystals of **3a** ($FeRuC_{15}H_{12}N_2O_6$, M_r = 473.2, Z = 4) are monoclinic, space group $P2_1/n$ and have cell constants a = 16.945(3), b = 13.796(6), c = 7.687(2) Å and β = 97.66(2)°. A total of 3174 reflections was used in the refinement which converged to a final R value of 0.038. Dark purple crystals of **4a** ($Fe_2RuC_{19}H_{12}N_2O_{10}$, M_r = 641.1, Z = 4) are monoclinic, space group $P2_1/a$ and have cell constants a = 14.800(2), b = 14.705(2), c = 11.034(1) Å and β = 92.87(2)°. A total of 4781 reflections was used in the refinement which converged to a final R value of 0.033. The carbonyl ligands of complexes **4a–c** were found to be involved in fluxional movements on the NMR timescale. From the spectroscopic data it can be concluded that several processes are occurring, of which the possible mechanisms are discussed.

Introduction**

α-Diimine ligands RN=CH-CH=NR (R-DAB) and C_5H_4N-2-CH=NR (R-Pyca) in transition metal complexes are known to show a versatile coordination behaviour, based on their ability to donate from 2 up to 8 electrons via the nitrogen lone pairs and the C=N π-electrons to one or more metal centres [1]. This versatility has led to a large body of interesting chemistry and a reasonable good understanding of the factors governing formation and properties of the α-diimine complexes [2–10]. In particular compounds containing the 6e bridging σ-N,μ_2-N',η^2-C=N' bonded α-diimine ligand proved to be excellent starting compounds for a host of unusual reactions with small molecules owing in many cases to the activation of the η^2-bonded imine moiety by the bimetallic core. The reactivity of the complexes $M_2(CO)_6(L)$ (M_2 = Fe_2, FeRu, Ru_2; L = R-DAB, R-Pyca), in which the α-diimine is bonded as a bridging σ-N,μ_2-N',η^2-C=N' six electron donor, towards small molecules like H_2, CO and unsaturated substrates such as R-DAB, R-Pyca, carbodiimines (RN=C=NR), sulfines (R_2C=S=O), ketene (H_2C=C=O), allene (H_2C=C=CH_2) and alkynes (RC≡CR') led to a rich chemistry involving C–C, C–H, C–N and N–H coupling reactions [1, 4, 5, 6, 8].

Although synthetic routes for the preparation of $Fe_2(CO)_6(L)$ (L = R-DAB, R-Pyca) [4–6] and $Ru_2(CO)_6(L)$ (L = R-DAB, R-Pyca) [4, 6] were known, as well as a synthetic route for the preparation of $FeRu(CO)_6$(R-DAB) [3], no synthetic pathway was available for the preparation of complexes $FeRu(CO)_6$(R-Pyca). Since the R-DAB ligand in $FeRu(CO)_6$(R-DAB) unexpectedly could be hydrogenated [7] and also showed an interesting reactivity towards

*Author to whom correspondence should be addressed.

**Abbreviations: R-DAB = 1,4-diaza-1,3-butadiene, R-N=CHCH=N-R; R-Pyca = pyridine-2-carbaldiimine, C_5H_4N-2-CH=N-R.

0020-1693/93/$6.00

alkynes [9, 10], it appeared worthwhile to attempt the synthesis of $FeRu(CO)_6$(R-Pyca) and compare its reactivity with that of $FeRu(CO)_6$(R-DAB).

In this article we present the synthesis of $FeRu(CO)_6$(R-Pyca) (**3a–c**), which was formed together with $Fe_2Ru(CO)_{10}$(R-Pyca) (**4a–c**), as well as an interesting fluxional behaviour that is observed for the carbonyl ligands of complexes **4a–c**. The reactivity of $FeRu(CO)_6$(R-Pyca) (**3a–c**) towards hydrogen and alkynes will be published separately [11, 12].

Experimental

Materials and apparatus

^1H and ^{13}C NMR spectra were recorded on Bruker AC-100 and AMX-300 spectrometers. IR spectra (ν(CO); 2200–1600 cm^{-1}) were measured on a Perkin-Elmer 283 spectrometer. Mass spectra were obtained on a Varian MAT 711 double focussing mass spectrometer with a combined EI/FI/FD ion source and coupled to a spectro system MAT 100 data acquisition unit [13]. Elemental analyses were carried out by the section elemental analyses of the Institute of Applied Chemistry TNO, Zeist, The Netherlands. All preparations were carried out under an atmosphere of purified nitrogen, using carefully dried solvents. Column chromatography was performed using silica gel (Kieselgel 60, Merck, 70–230 Mesh ASTM, dried and activated before use) as the stationary phase. $Ru_3(CO)_{12}$ (Strem) was used as commercially obtained. $Ru_2(CO)_4$(R-Pyca)$_2$ (**1a–c**) [14], $Fe_2(CO)_9$ (**2**)* and $Ru_2(CO)_4$(^{i}Pr-DAB)$_2$ [4] were prepared according to literature procedures.

Synthesis of FeRu(CO)(R-Pyca) (3a–c) and $Fe_2Ru(CO)_{10}$(R-Pyca) (4a–c) by reaction of $Ru_2(CO)_4$(R-Pyca)$_2$ (1) with $Fe_2(CO)_9$ (2)

An amount of 1.0 mmol $Ru_2(CO)_4$(R-Pyca)$_2$ (R = ^{i}Pr (**1a**); R = ^{c}Hex (**1b**); R = ^{t}Bu (**1c**)) was suspended in 75 ml of solvent (toluene, THF, Et_2O) and treated with $Fe_2(CO)_9$ (**2**) in portions of 0.5 g (1.37 mmol) at room temperature. Every new portion was added when no solid $Fe_2(CO)_9$ from the previous portion was left in the reaction mixture. During the reaction the color of the mixture changed from yellow to dark brown–purple and the reaction was stopped when IR spectroscopy indicated that all **1** had been consumed. The mixture was then evaporated to dryness to remove the $Fe(CO)_5$ formed**, and the residue was extracted with hexane (in portions of 50 ml) until the extract became almost colorless. The resulting residue was extracted with CH_2Cl_2 (3×50 ml) affording a dark purple extract.

The dark green hexane extract, which contained $FeRu(CO)_6$(R-Pyca) (R = ^{i}Pr (**3a**); R = ^{c}Hex (**3b**); R = ^{t}Bu (**3c**)) and $Fe_3(CO)_{12}$** was evaporated to dryness, dissolved in 50 ml heptane and refluxed until IR spectroscopy indicated that all $Fe_3(CO)_{12}$ had decomposed†, leaving only complex **3** in solution. The warm solution was filtered over celite, leaving pyrophoric Fe powder behind. Upon keeping the filtrate at −20 °C overnight, complex **3** precipitated as red crystals suitable for an X-ray single crystal structure determination.

The purple CH_2Cl_2 extract was filtered over celite, concentrated to 10 ml and purified by column chromatography. Elution with ligroin afforded a green fraction which contained $Fe_3(CO)_{12}$. Elution with ligroin/CH_2Cl_2 (1/1) resulted in a yellow fraction containing small amounts of unreacted $Ru_2(CO)_4$(R-Pyca)$_2$ (**1**). Finally, elution with CH_2Cl_2 afforded a dark purple fraction containing $Fe_2Ru(CO)_{10}$(R-Pyca) (R = ^{i}Pr (**4a**); R = ^{c}Hex (**4b**); R = ^{t}Bu (**4c**)). Subsequent crystallization from hexane/CH_2Cl_2 at −20 °C yielded dark purple crystals suitable for an X-ray single crystal structure determination.

Thermal conversion of $Fe_2Ru(CO)_{10}$(R-Pyca) (4a–c) to $FeRu(CO)_6$(R-Pyca) (3a–c)

A solution of 0.33 mmol of $Fe_2Ru(CO)_{10}$(R-Pyca) (R = ^{i}Pr (**4a**); R = ^{c}Hex (**4b**); R = ^{t}Bu (**4c**)) in 50 ml toluene was stirred at 70 °C until IR spectroscopy indicated that complex **4** was completely converted to **3** (about 1.5 h). The solution was then filtered over celite, evaporated to dryness and the residue was purified by column chromatography. Elution with ligroin/CH_2Cl_2 (9/1) afforded an orange–red fraction that contained complex **3** in more than 90% yield.

Reaction of $Ru_2(CO)_4$(R-Pyca)$_2$ (1a–c) with $Ru_3(CO)_{12}$ to give $Ru_2(CO)_6$(R-Pyca)

An amount of 0.2 mmol $Ru_2(CO)_4$(R-Pyca)$_2$ (R = ^{i}Pr (**1a**); R = ^{c}Hex (**1b**); R = ^{t}Bu (**1c**)) was dissolved in toluene (40 ml) and 0.3 mmol $Ru_3(CO)_{12}$ was added. The mixture was stirred at 100 °C until IR spectroscopy indicated that complex **1** had been consumed (about

*$Fe_2(CO)_9$ was prepared by a slightly modified literature procedure using a quartz Schlenk tube and starting with 25 ml $Fe(CO)_5$, 150 ml glacial acetic acid and 10 ml acetic anhydride (the latter was added to prevent the mixture containing too much water). A Rayonet RS photochemical reactor (λ_{max} = 2500 Å) was used for irradiation and a continuous stream of air was used to cool the reaction mixture. Filtration, washing with water, ethanol and pentane and subsequently drying *in vacuo* gave $Fe_2(CO)_9$ in usually more than 90% yield (see also ref. 15).

$Fe(CO)_5$ is formed as a side product from $Fe_2(CO)_9$ via $Fe_2(CO)_9 \rightarrow Fe(CO)_5 + Fe(CO)_4$. The $Fe(CO)_4$ fragments that do not react with **1 trimerize forming $Fe_3(CO)_{12}$. For more information about this behaviour see ref. 16.

†The thermal instability of $Fe_3(CO)_{12}$ in solution at temperatures above 60 °C is well established (see ref. 17).

2.5 h). The reaction mixture was then evaporated to dryness, the residue was dissolved in a minimum amount of CH_2Cl_2 and purified by column chromatography. Elution with ligroin afforded two yellow fractions. The first fraction contained unreacted $Ru_3(CO)_{12}$ while the second fraction afforded $Ru_2(CO)_6$(R-Pyca) [5, 6] in 35–40% yield.

Reaction of $Ru_2(CO)_4$(^{i}Pr-DAB)$_2$ with $Fe_2(CO)_9$ to give $FeRu(CO)_6$(^{i}Pr-DAB)

In a typical experiment 500 mg of $Ru_2(CO)_4$(^{i}Pr-DAB)$_2$ (0.84 mmol) was dissolved in 75 ml toluene and treated with $Fe_2(CO)_9$ in portions of 0.5 g (1.37 mmol) at reflux temperature. Each new portion was added when no solid $Fe_2(CO)_9$ from the previous portion was left in the reaction mixture. After 70 h the reaction was stopped and the reaction mixture was evaporated to dryness. The residue was dissolved in a minimum amount of CH_2Cl_2 and purified by column chromatography. Elution with ligroin/CH_2Cl_2 (9/1) afforded an orange–red fraction which contained $FeRu(CO)_6$(^{i}Pr-DAB) as evidenced by its IR and NMR data [3]. Elution with ligroin/CH_2Cl_2 (1/1) gave a yellow fraction that contained the unreacted $Ru_2(CO)_4$(^{i}Pr-DAB)$_2$ (about 0.25 g). The yield of the reaction was about 5% (10% based on the $Ru_2(CO)_4$(^{i}Pr-DAB)$_2$ consumed).

*Crystal structure determination of $FeRu(CO)_6$(^{i}Pr-Pyca) (**3a**)*

The crystallographic data of **3a** are listed in Table 1. The reflections were measured on an Enraf-Nonius CAD-4 diffractometer (293 K, 0–2θ scan) with graphite-monochromated Mo Kα radiation. The reflections with an intensity below 2.5$\sigma(I)$ were treated as not observed. The maximum value of sin θ/λ was 0.70 A^{-1}. Unit-cell parameters were refined by a least-squares fitting procedure using 23 reflections with $38 \leqslant 2\theta \leqslant 42°$. Corrections for Lorentz and polarization effects were applied. The positions of the Fe and Ru atom were determined by direct methods with the program SIMPEL [18]. The rest of the non-hydrogen atoms were derived from a ΔF synthesis. After isotropic refinement the H atoms were derived from subsequent ΔF synthesis. Block-diagonal least-squares refinement on F, anisotropic for the non-hydrogen atoms and isotropic for the hydrogen atoms, converged to $R = 0.038$, $R_w = 0.066$, $(\Delta\sigma)_{max} = 0.93$, $w = (5.08 + F_{obs} + 0.015F_{obs}^2)^{-1}$. An empirical absorption correction (DIFABS) [19] was applied, with coefficients in the range 0.75–1.17. A final difference Fourier map revealed a residual electron density between -0.6 and 0.6 e $Å^{-3}$. Scattering factors were taken from Cromer and Mann [20, 21]. Anomalous dispersion for Fe and Ru were taken into account. All calculations were performed with XRAY76 [22].

*Crystal structure determination of $Fe_2Ru(CO)_{10}$(^{i}Pr-Pyca) (**4a**)*

The crystallographic data of **4a** are listed in Table 1. The reflections were measured on an Enraf-Nonius CAD-4 diffractometer (293 K, 0–2θ scan) with graphite-monochromated Mo Kα radiation. The reflections with an intensity below 2.5$\sigma(I)$ were treated as not observed. The maximum value of sin θ/λ was 0.70 A^{-1}. Unit-cell parameters were refined by a least-squares fitting procedure using 23 reflections with $38 \leqslant 2\theta \leqslant 40°$. Corrections for Lorentz and polarization effects were applied. The positions of the Fe and Ru atom were determined by direct methods with the program SIMPEL [18]. The rest of the non-hydrogen atoms were derived from a ΔF synthesis. After isotropic refinement the H atoms were derived from subsequent ΔF synthesis. Block-diagonal least-squares refinement on F, anisotropic for the non-hydrogen atoms and isotropic for the hydrogen atoms, converged to $R = 0.033$, $R_w = 0.058$, $(\Delta/\sigma)_{max} = 0.83$, $w = (4.74 + F_{obs} + 0.012F_{obs}^2)^{-1}$. An empirical absorption correction (DIFABS) [19] was applied, with coefficients in the range of 0.82–1.15. A final difference Fourier map revealed a residual electron density between -0.3 and 0.4 e $Å^{-3}$. Scattering factors were taken from Cromer and Mann [20, 21]. Anomalous dispersion for Fe and Ru were taken into account. All calculations were performed with XRAY76 [22].

Results and discussion

*Formation of complexes **3a–c** and **4a–c***

The new complexes $FeRu(CO)_6$(R-Pyca) (**3a–c**) and $Fe_2Ru(CO)_{10}$(R-Pyca) (**4a–c**) were obtained by reaction of $Ru_2(CO)_4$(R-Pyca)$_2$ with $Fe_2(CO)_9$ at room temperature. Complexes **4a–c** proved to be thermally unstable and converted to **3a–c** by heating at 70 °C. The observed reaction sequence and the structures of the new complexes are schematically presented in Scheme 1. In the following we will first discuss the spectroscopic and structural data of the relevant complexes and subsequently deal with aspects of their formation and their properties.

*Molecular structure of **3a***

A view [23] of the molecular structure of **3a** is shown in Fig. 1, while Table 2 contains the fractional coordinates of the non hydrogen atoms. The bond distances and bond angles of the non-hydrogen atoms of **3a** are listed in Tables 3 and 4, respectively.

As shown in Fig. 1 the molecule contains an Fe–Ru bond with a length of 2.653(3) Å, which is comparable to the Fe–Ru bond length in $FeRu(CO)_6$(^{i}Pr-DAB) (2.6602(9) Å) [3]. This is a normal value for an Fe–Ru bond, which usually varies from 2.60 to 2.80 Å with

TABLE 1. Crystallographic data for $FeRu(CO)_6$(^{i}Pr-Pyca) (**3a**) and $Fe_2Ru(CO)_{10}$(^{i}Pr-Pyca) (**4a**)

	3a	**4a**
Crystal data		
Formula	$FeRuC_{15}H_{12}N_2O_6$	$Fe_2RuC_{19}H_{12}N_2O_{10}$
Molecular weight	473.2	641.08
Crystal system	monoclinic	monoclinic
Space group	$P2_1/n$	$P2_1/a$
a (Å)	16.945(3)	14.800(2)
b (Å)	13.796(6)	14.705(1)
c (Å)	7.678(2)	11.034(1)
β (°)	97.66(2)	92.87(2)
V (Å^3)	1781(1)	2398.4(7)
D_{calc} (g cm^{-3})	1.77	1.78
Z	4	4
$F(000)$	936	1264
μ (cm^{-1})	16.78	18.6
Crystal size (mm)	0.17×0.17×0.5	0.3×0.3×0.35
Data collection		
Temperature (K)	295	295
Radiation	Mo Kα	Mo Kα
$\theta_{min}/\theta_{max}$ (°)	2.5, 30	2.5, 30
Scan type	$\omega/2\theta$	$\omega/2\theta$
$\Delta\omega$ (°)	1.1+0.15 tan(θ)	0.9+0.35 tan(θ)
Horizontal and vertical aperture (mm)	3.577, 4.00	3.577, 4.00
Reference reflections	3 3 0; $\bar{4}$ 1 2	4 1 0; $\bar{1}$ 4 2
Data set	h −23:23; k 0:19; l 0:10	h −20:20; k 0:20; l 0:15
Total data	5434	7290
Unique data	5150	6937
Observed data ($I>2.5\sigma(I)$)	3174	4781
Refinement		
Refined parameters	386	495
R, R_w	0.038, 0.066	0.033, 0.058
Weighting scheme, w	$(5.08+F_{obs}+0.015F_{obs}^2)^{-1}$	$(4.74+F_{obs}+0.012F_{obs}^2)^{-1}$
Absorption correction	DIFABS	DIFABS
Max./min. residual density (e Å^{-3})	0.6, −0.6	0.4, −0.3

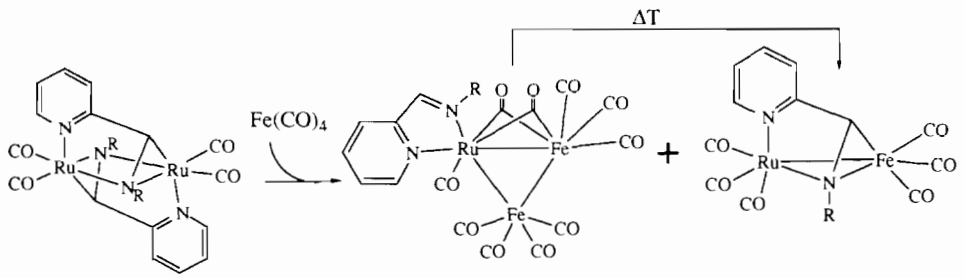

R = ^{i}Pr (**1a**) R = ^{i}Pr (**4a**) R = ^{i}Pr (**3a**)
R = ^{c}Hex (**1b**) R = ^{c}Hex (**4b**) R = ^{c}Hex (**3b**)
R = ^{t}Bu (**1c**) R = ^{t}Bu (**4c**) R = ^{t}Bu (**3c**)

Scheme 1. Observed reaction sequence for the preparation of complexes **3a–c** and **4a–c.**

the average being approximately 2.69 Å [24, 25]. The metal carbonyl part of the structure consists of three carbonyl groups terminally bonded to Fe (Fe–C(O) = 1.780 Å (mean)) and three carbonyl groups terminally bonded to Ru (Ru–C(O) = 1.920 Å (mean)). The Ru–C(11) bond of the CO ligand *trans* to the σ-coordinated N(2) nitrogen is shortened (1.901(5) Å) as a result of this *trans* influence.

The Pyca ligand is coordinated to the Ru centre via N(1) and N(2) and the Fe centre via η^2-coordination

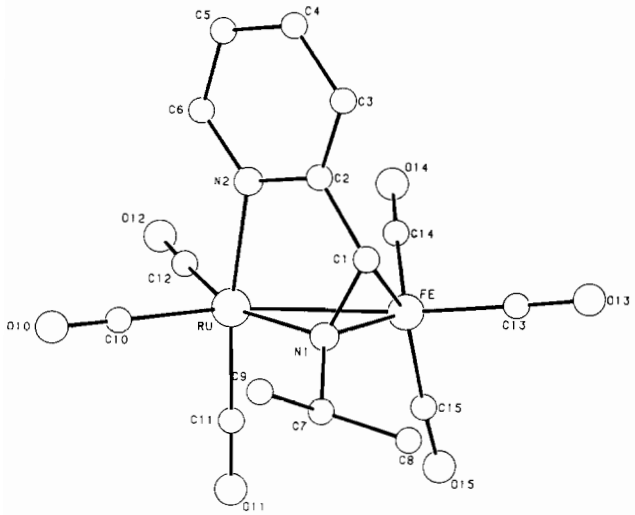

Fig. 1. Pluto drawing of $FeRu(CO)_6(^iPr\text{-}Pyca)$ (**3a**).

TABLE 2. Fractional coordinates and equivalent isotropic thermal parameters of the non-hydrogen atoms of $FeRu(CO)_6(^iPr\text{-}Pyca)$ (**3a**) with e.s.d.s in parentheses

	x	*y*	*z*	U_{eq}
Ru	0.34427(2)	0.31479(3)	0.80034(5)	0.0409(2)
Fe	0.46914(4)	0.25335(5)	1.01747(9)	0.0427(4)
C1	0.4075(3)	0.1337(4)	0.9180(8)	0.050(3)
C2	0.3272(3)	0.1289(4)	0.9680(7)	0.046(3)
C3	0.2975(4)	0.0496(5)	1.0527(8)	0.062(4)
C4	0.2200(5)	0.0555(6)	1.0969(10)	0.077(5)
C5	0.1752(4)	0.1362(6)	1.053(1)	0.077(5)
C6	0.2067(4)	0.2114(5)	0.9653(9)	0.060(3)
C7	0.4638(4)	0.1737(5)	0.6392(8)	0.060(3)
C8	0.5415(5)	0.1238(6)	0.687(1)	0.081(5)
C9	0.4073(4)	0.1152(5)	0.5128(8)	0.067(4)
C10	0.2707(4)	0.3035(5)	0.5840(8)	0.059(3)
C11	0.4122(4)	0.4063(4)	0.7099(8)	0.056(3)
C12	0.2893(4)	0.4185(5)	0.8977(9)	0.061(4)
C13	0.5420(4)	0.1791(5)	1.1348(8)	0.057(3)
C14	0.4187(4)	0.3079(4)	1.1830(8)	0.055(3)
C15	0.5397(4)	0.3463(5)	0.9863(9)	0.064(4)
N1	0.4240(3)	0.2014(3)	0.7933(6)	0.042(2)
N2	0.2816(3)	0.2080(4)	0.9242(6)	0.047(2)
O10	0.2277(3)	0.2972(4)	0.4579(7)	0.082(3)
O11	0.4526(3)	0.4601(4)	0.6526(8)	0.084(4)
O12	0.2575(3)	0.4778(4)	0.9605(9)	0.098(4)
O13	0.5885(3)	0.1269(4)	1.2121(8)	0.082(3)
O14	0.3889(3)	0.3436(4)	1.2911(6)	0.079(3)
O15	0.5866(4)	0.4048(5)	0.9745(9)	0.103(4)

of the C(1)=N(1) imine bond. Coordination to the Fe centre elongates the C(1)=N(1) imine bond significantly (1.393(5) Å) as compared for instance to the value of 1.258(3) Å in the case of free ^cHex-DAB [26] and is similar to the length of the η^2-bonded C=N moiety in $Fe_2(CO)_6(^cHex\text{-}DAB)$ for which a value of 1.397(4) Å was found [5, 6]. The lengthening of this imine bond has been explained by π-backbonding from the Fe atom

TABLE 3. Bond distances (Å) of the non-hydrogen atoms of $FeRu(CO)_6(^iPr\text{-}Pyca)$ (**3a**) with e.s.d.s in parentheses

Ru–Fe	2.653(3)	Fe–N1	1.928(4)	C7–C8	1.488(8)
Ru–C10	1.947(5)	C1–C2	1.464(6)	C7–C9	1.505(7)
Ru–C11	1.901(5)	C1–N1	1.393(5)	C7–N1	1.489(6)
Ru–C12	1.913(5)	C2–C3	1.400(6)	C10–O10	1.136(6)
Ru–N1	2.072(4)	C2–N2	1.353(5)	C11–O11	1.137(6)
Ru–N2	2.115(4)	C3–C4	1.402(8)	C12–O12	1.123(7)
Fe–C1	2.046(4)	C4–C5	1.364(8)	C13–O13	1.170(6)
Fe–C13	1.758(5)	C5–C6	1.383(8)	C14–O14	1.140(6)
Fe–C14	1.790(5)	C6–N2	1.349(6)	C15–O15	1.145(7)
Fe–C15	1.791(6)				

TABLE 4. Bond angles (°) of the non-hydrogen atoms of $FeRu(CO)_6(^iPr\text{-}Pyca)$ (**3a**) with e.s.d.s in parentheses

Fe–Ru–C10	151.4(2)	Fe–C1–C2	112.6(4)
Fe–Ru–C11	88.4(2)	Fe–C1–N1	65.0(3)
Fe–Ru–C12	112.4(2)	C2–C1–N1	119.3(4)
Fe–Ru–N1	46.2(1)	C1–C2–C3	124.2(5)
Fe–Ru–N2	84.3(2)	C1–C2–N2	114.7(5)
C10–Ru–C11	95.2(3)	C3–C2–N2	121.1(5)
C10–Ru–C12	96.0(3)	C2–C3–C4	118.3(5)
C10–Ru–N1	105.2(3)	C3–C4–C5	119.7(6)
C10–Ru–N2	91.5(3)	C4–C5–C6	119.6(7)
C11–Ru–C12	89.8(3)	C5–C6–N2	121.6(5)
C11–Ru–N1	93.6(3)	C8–C7–C9	112.2(6)
C11–Ru–N2	172.6(2)	C8–C7–N1	113.7(5)
C12–Ru–N1	158.1(2)	C9–C7–N1	109.6(5)
C12–Ru–N2	92.6(3)	Ru–C10–O10	179.8(4)
N1–Ru–N2	81.6(2)	Ru–C11–O11	178.6(4)
Ru–Fe–C1	72.4(2)	Ru–C12–O12	177.5(4)
Ru–Fe–C13	162.9(2)	Fe–C13–O13	177.5(4)
Ru–Fe–C14	84.1(3)	Fe–C14–O14	177.8(4)
Ru–Fe–C15	100.2(3)	Fe–C15–O15	176.6(4)
Ru–Fe–N1	50.8(2)	Ru–N1–Fe	83.0(2)
C1–Fe–C13	90.6(3)	Ru–N1–C1	107.3(3)
C1–Fe–C14	109.7(3)	Ru–N1–C7	125.5(3)
C1–Fe–C15	147.6(2)	Fe–N1–C1	74.1(3)
C1–Fe–N1	40.9(2)	Fe–N1–C7	129.7(3)
C13–Fe–C14	104.4(4)	C1–N1–C7	121.9(4)
C13–Fe–C15	92.9(4)	Ru–N2–C2	111.7(3)
C13–Fe–N1	114.2(3)	Ru–N2–C6	128.7(3)
C14–Fe–C15	100.6(4)	C2–N2–C6	119.6(5)
C14–Fe–N1	128.4(3)		
C15–Fe–N1	109.8(3)		

into the π^*-orbital of the C=N double bond [1, 27]. The N(2)–C(2) distance of 1.353(5) Å of the σ-N coordinated pyridine ring is significantly larger than the distance of the σ-N coordinated imine bond in $FeRu(CO)_6(^iPr\text{-}DAB)$ (1.296(6) Å) [3], which is probably due to delocalization of electron density within the pyridine ring. Usually the planarity of the N=C–C=N system of an α-diimine ligand is not affected significantly by σ-N,μ_2-N′,η^2-C=N′ coordination [4, 5, 6, 14, 27]. The torsion angle between the N(1)–C(1) bond and the N(2)–C(2) bond in **3a** is 17° as can be seen from Fig. 2. This is one of the largest values

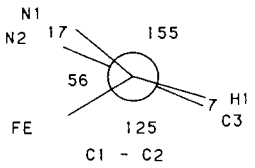

Fig. 2. Newman projection along the C(1)–C(2) bond of $FeRu(CO)_6(^iPr\text{-}Pyca)$ (**3a**).

reported so far as compared, for example, to the angles in $Ru_2(CO)_4(R\text{-}Pyca)_2$ (6°) [14], $Ru_2(CO)_4(R\text{-}DAB)_2$ (6°) [4], $MnCo(CO)_6(DAB)$ (11°) [27], $Fe_2(CO)_6(^cHex\text{-}DAB)$ (12°) [5] or $FeRu(CO)_6(^iPr\text{-}DAB)$ (13°) [28], $FeRu(H)(Me)(CO)_5(^iPr\text{-}DAB)$ (14.2°) [29] and $FeRu(CO)_4(PPh_3)_2(^iPr\text{-}Pyca)$ (22°) [11]. It seems that relatively large distortions are observed when the α-diimine ligand is coordinated to two metals that substantially differ in size.

Molecular structure of ***4a***

A view [23] of the molecular structure of **4a** is shown in Fig. 3, while Table 5 contains the fractional coordinates of the non hydrogen atoms. The bond distances and bond angles of the non-hydrogen atoms of **4a** are listed in Tables 6 and 7, respectively.

The molecule consists of a triangle of metal atoms with the ^iPr-Pyca ligand coordinated to the Ru centre via the lone pairs of the two nitrogen atoms. The plane of ^iPr-Pyca ligand N(1)C(1)C(2)C(3)C(4)C(5)C(6)N(2), which is virtually flat, is almost perpendicular to the plane of the metal triangle RuFe(1)Fe(2) (86.53°). The molecule contains eight terminal and two bridging carbonyls. Despite the fact that Ru has a larger covalent radius then Fe the latter two are closer to the Ru centre (1.983(3), 1.978(3) Å) than to the Fe centre (2.068(3), 2.043(3) Å), indicating that the two bridging carbonyls can best be regarded as bonded to the Ru centre and bridging to the Fe centre. Since the C–O vectors are approximately perpendicular to the Fe(1)–Ru vector (88.15 and 88.09°, respectively) these carbonyls can better be regarded as asymmetrically bridging rather than semi bridging [30].

It is interesting to note that the related cluster $Ru_3(CO)_{10}(Bipy)$ also possesses two bridging carbonyls [31, 32] whereas the unsubstituted $Ru_3(CO)_{12}$ does not [33], which agrees with the observation that an increased electron density on the metal core leads to an increased tendency to form bridging carbonyl ligands [24, 34–36]. The unsubstituted $Fe_2Ru(CO)_{12}$ also contains bridging carbonyl ligands [24, 37], and since upon substitution of two carbonyl ligands for a Pyca ligand the electron density on the metal core is raised, the presence of bridging carbonyl groups for **4** is as expected. The observation that the analogous $Os_3(CO)_{10}(^iPr\text{-}DAB)$ only has terminal carbonyls [38] is probably due to the DAB ligand being a better π-acceptor than R-Pyca or Bipy [1], thus lowering the electron density on the metal core. Furthermore carbonyl ligands generally prefer terminal positions in complexes of the third row transition metals [38].

As seen before in this type of complex [34, 38, 39] the axial carbonyl ligands on Fe(2) have a tendency to bend inwards above the metal triangle (RuFe(2)C(17) = 86.7(2)°, Fe(1)Fe(2)C(17) = 86.3(2)°, Fe(1)Fe(2)C(19) = 87.7(2)°, RuFe(2)C(19) = 82.4(2)°). The effect however is small and almost symmetrical, neither favouring Ru nor Fe(1), indicating that they should be regarded as terminally coordinated to Fe(2).

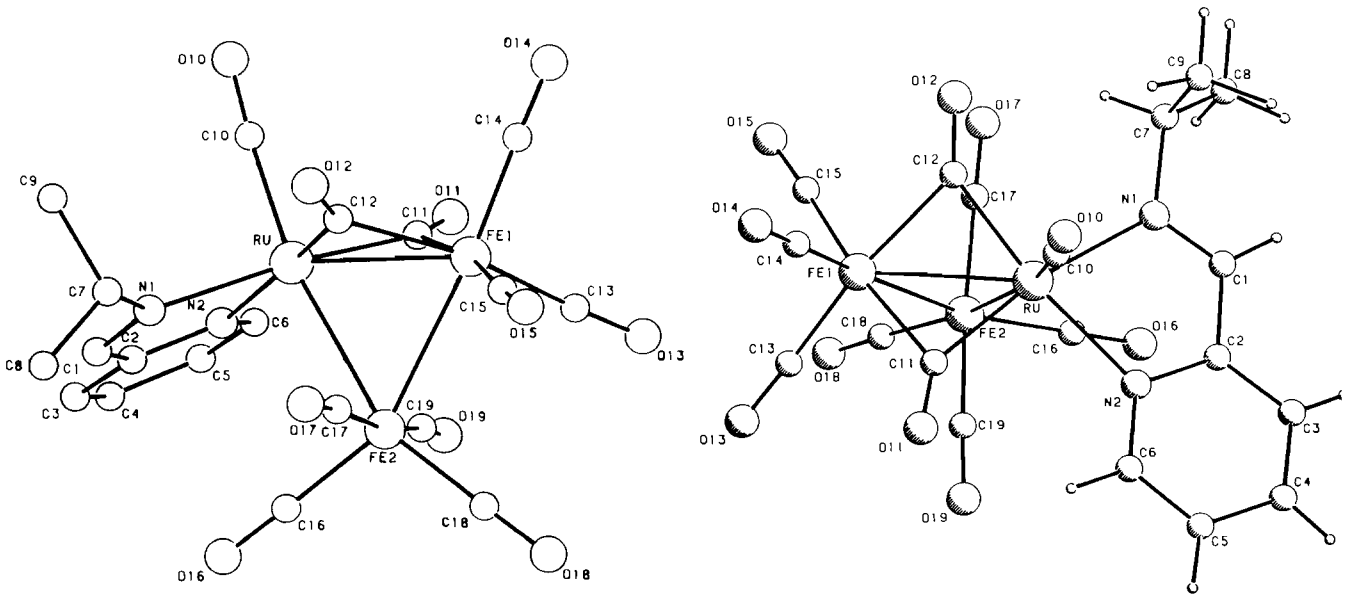

Fig. 3. Pluto drawing of two different views of $Fe_2Ru(CO)_{10}(^iPr\text{-}Pyca)$ (**4a**).

TABLE 5. Fractional coordinates and equivalent isotropic thermal parameters of the non-hydrogen atoms of $Fe_2Ru(CO)_{10}$(^{i}Pr-Pyca) (**4a**) with e.s.d.s in parentheses

	x	y	z	U_{eq}
Ru	0.33952(2)	0.43000(2)	0.28687(2)	0.0368(1)
Fe1	0.28196(4)	0.29629(4)	0.14540(5)	0.0423(3)
Fe2	0.17972(4)	0.44894(4)	0.14841(7)	0.0532(3)
C1	0.3045(3)	0.5892(3)	0.4414(4)	0.057(2)
C2	0.3564(3)	0.6297(3)	0.3468(3)	0.043(2)
C3	0.3817(3)	0.7203(3)	0.3484(4)	0.055(2)
C4	0.4355(4)	0.7523(3)	0.2615(5)	0.065(3)
C5	0.4639(4)	0.6933(3)	0.1743(5)	0.064(3)
C6	0.4371(3)	0.6032(3)	0.1771(4)	0.052(2)
C7	0.2470(6)	0.4616(4)	0.5459(5)	0.101(5)
C8	0.1784(9)	0.5172(6)	0.5999(10)	0.180(10)
C9	0.321(1)	0.4393(8)	0.6395(7)	0.18(1)
C10	0.4494(4)	0.3949(4)	0.3688(4)	0.063(3)
C11	0.3876(3)	0.3872(3)	0.1323(3)	0.044(2)
C12	0.2859(3)	0.3118(3)	0.3296(4)	0.052(2)
C13	0.2714(4)	0.3036(3)	−0.0169(4)	0.062(3)
C14	0.3565(4)	0.2012(3)	0.1517(5)	0.061(3)
C15	0.1797(4)	0.2322(4)	0.1663(5)	0.066(3)
C16	0.1507(4)	0.5597(4)	0.2005(6)	0.77(4)
C17	0.1249(4)	0.3977(4)	0.2726(6)	0.077(4)
C18	0.0940(3)	0.4223(4)	0.0328(6)	0.071(3)
C19	0.2536(4)	0.4972(4)	0.0421(5)	0.068(3)
N1	0.2901(3)	0.5040(3)	0.4397(3)	0.056(2)
N2	0.3833(2)	0.5707(2)	0.2615(3)	0.041(2)
O10	0.5142(3)	0.3687(4)	0.4141(5)	0.121(4)
O11	0.4434(2)	0.4009(3)	0.0646(3)	0.064(2)
O12	0.2669(3)	0.2677(2)	0.4126(3)	0.077(2)
O13	0.2666(4)	0.3043(4)	−0.1198(4)	0.103(3)
O14	0.4023(3)	0.1393(3)	0.1544(5)	0.102(3)
O15	0.1182(3)	0.1888(3)	0.1773(6)	0.114(4)
O16	0.1340(4)	0.6296(3)	0.2350(6)	0.119(4)
O17	0.0843(4)	0.3684(4)	0.3499(5)	0.112(4)
O18	0.0415(3)	0.4066(4)	−0.0434(5)	0.100(3)
O19	0.2952(3)	0.5333(4)	−0.0281(5)	0.100(3)

TABLE 6. Bond distances (Å) of the non-hydrogen atoms of $Fe_2Ru(CO)_{10}$(^{i}Pr-Pyca) (**4a**) with e.s.d.s in parentheses

Ru–Fe1	2.6259(8)	Fe2–C16	1.787(4)	C7–C9	1.50(1)
Ru–Fe2	2.7646(9)	Fe2–C17	1.793(5)	C7–N1	1.498(5)
Ru–C10	1.892(4)	Fe2–C18	1.797(4)	C10–O10	1.127(5)
Ru–C11	1.983(3)	Fe2–C19	1.790(4)	C11–O11	1.159(4)
Ru–C12	1.978(3)	C1–C2	1.454(4)	C12–O12	1.168(4)
Ru–N1	2.165(3)	C1–N1	1.271(4)	C13–O13	1.134(4)
Ru–N2	2.190(2)	C2–C3	1.384(4)	C14–O14	1.134(5)
Fe1–Fe2	2.7082(9)	C2–N2	1.354(4)	C15–O15	1.123(5)
Fe1–C11	2.068(3)	C3–C4	1.361(5)	C16–O16	1.128(5)
Fe1–C12	2.043(3)	C4–C5	1.377(5)	C17–O17	1.151(6)
Fe1–C13	1.793(3)	C5–C6	1.384(5)	C18–O18	1.140(5)
Fe1–C14	1.780(3)	C6–N2	1.343(4)	C19–O19	1.144(5)
Fe1–C15	1.807(4)	C7–C8	1.454(10)		

TABLE 7. Bond angles (°) of the non-hydrogen atoms of $Fe_2Ru(CO)_{10}$(^{i}Pr-Pyca) (**4a**) with e.s.d.s in parentheses

Fe1–Ru–Fe2	60.25(4)	Ru–Fe2–C17	86.7(2)
Fe1–Ru–C10	109.0(2)	Ru–Fe2–C18	157.6(1)
Fe1–Ru–C11	51.0(1)	Ru–Fe2–C19	82.4(2)
Fe1–Ru–C12	50.3(1)	Fe1–Fe2–C16	154.6(1)
Fe1–Ru–N1	136.66(8)	Fe1–Fe2–C17	86.3(2)
Fe1–Ru–N2	136.10(7)	Fe1–Fe2–C18	100.7(2)
Fe2–Ru–C10	169.2(1)	Fe1–Fe2–C19	87.7(2)
Fe2–Ru–C11	83.7(1)	C16–Fe2–C17	90.7(3)
Fe2–Ru–C12	83.0(1)	C16–Fe2–C18	104.7(3)
Fe2–Ru–N1	93.8(1)	C16–Fe2–C19	90.8(3)
Fe2–Ru–N2	94.85(10)	C17–Fe2–C18	96.9(3)
C10–Ru–C11	89.3(2)	C17–Fe2–C19	169.1(2)
C10–Ru–C12	89.5(2)	C18–Fe2–C19	93.1(3)
C10–Ru–N1	94.6(2)	C2–C1–N1	119.2(3)
C10–Ru–N2	93.8(2)	C1–C2–C3	122.5(3)
C11–Ru–C12	95.3(2)	C1–C2–N2	114.9(3)
C11–Ru–N1	168.3(1)	C3–C2–N2	122.5(3)
C11–Ru–N2	93.9(2)	C2–C3–C4	119.4(4)
C12–Ru–N1	95.8(2)	C3–C4–C5	119.0(4)
C12–Ru–N2	170.3(1)	C4–C5–C6	119.3(4)
N1–Ru–N2	74.8(1)	C5–C6–N2	122.5(3)
Ru–Fe1–Fe2	62.41(4)	C8–C7–C9	109.9(8)
Ru–Fe1–C11	48.20(10)	C8–C7–N1	114.8(6)
Ru–Fe1–C12	48.1(1)	C9–C7–N1	107.7(6)
Ru–Fe1–C13	123.9(1)	Ru–C10–O10	175.6(3)
Ru–Fe1–C14	112.5(2)	Ru–C11–Fe1	80.8(2)
Ru–Fe1–C15	124.3(2)	Ru–C11–O11	142.9(2)
Fe2–Fe1–C11	83.7(1)	Fe1–C11–O11	136.3(2)
Fe2–Fe1–C12	83.3(1)	Ru–C12–Fe1	81.5(2)
Fe2–Fe1–C13	86.7(2)	Ru–C12–O12	142.2(2)
Fe2–Fe1–C14	174.9(1)	Fe1–C12–O12	136.2(2)
Fe2–Fe1–C15	87.6(2)	Fe1–C13–O13	176.8(3)
C11–Fe1–C12	90.8(2)	Fe1–C14–O14	178.3(3)
C11–Fe1–C13	85.4(2)	Fe1–C15–O15	176.7(3)
C11–Fe1–C14	92.4(2)	Fe2–C16–O16	178.5(3)
C11–Fe1–C15	170.7(2)	Fe2–C17–O17	175.1(3)
C12–Fe1–C13	169.6(2)	Fe2–C18–O18	177.7(3)
C12–Fe1–C14	93.6(2)	Fe2–C19–O19	174.2(3)
C12–Fe1–C15	85.0(2)	Ru–N1–C1	116.4(3)
C13–Fe1–C14	96.3(2)	Ru–N1–C7	125.0(3)
C13–Fe1–C15	97.3(2)	C1–N1–C7	118.5(4)
C14–Fe1–C15	96.1(3)	Ru–N2–C2	114.7(2)
Ru–Fe2–Fe1	57.33(4)	Ru–N2–C6	127.9(2)
Ru–Fe2–C16	97.3(2)	C2–N2–C6	117.3(3)

Many examples have been published of complexes derived from $M_3(CO)_{12}$ by substitution of one or more carbonyl ligands by phosphorous or nitrogen ligands [24, 34, 39–44]. It should be noted that substitution of CO by more bulky ligands results in the latter occupying the sterically least demanding sites, which in all cases is the equatorial one [24, 34, 39, 40]. Only ligands smaller than CO such as nitriles [41] or isonitriles [42] occupy the axial sites in $M_3(CO)_{12-n}(L)_n$ complexes. In all other cases the substituting ligand prefers an equatorial position, even in the case of tetra or penta substitution [34, 43] or in the case of a bidentate phosphine ligand [44].

In complex **4a** the angles of the Ru–N(1) bond and the Ru–N(2) bond with the plane of the metal triangle are 36.7 and 38.2°, respectively, indicating that N(1) is positioned about just as much above the plane of the metal triangle (1.29 Å) as N(2) is positioned below

this plane (1.35 Å). Alternatively one might say that the ^{i}Pr-Pyca ligand occupies a pseudo equatorial position since both nitrogen atoms are at the same distance from this equatorial plane. The same type of coordination has been found for $Ru_3(CO)_{10}$(Bipy) [31, 32]. Why on the other hand in the case of $Os_3(CO)_{10}$(^{i}Pr-DAB) [38] one of the nitrogen atoms occupies an axial position and the other one an equatorial position is not clear. It might be that in the case of **4a–c** the bridging carbonyls force the α-diimine ligand into a pseudo equatorial position, as for $Ru_3(CO)_{10}$(Bipy) [31, 32].

The Ru–Fe(1) distance (2.6259(8) Å) is significantly shorter than the Ru–Fe(2) distance (2.7646(9) Å) which is probably due to the presence of the two bridging carbonyls which are known to have a shortening effect on a metal–metal bond [24, 31, 32, 34].

IR spectroscopy, mass spectroscopy and analyses

The IR spectroscopic data are listed in Table 8 together with the mass spectroscopic data and the results of the elemental analyses. The absorptions of the terminally bonded carbonyl ligands are observed as expected within the range 1900–2070 cm^{-1}. The bridging carbonyl ligands of the complexes **4** absorb between 1760 and 1785 cm^{-1}.

From the measurements of the mass spectra of the complexes **4a–c** it appeared that usually the experimental conditions were too severe to observe the molecular ion. In most cases the strongest signal in the spectrum was 168 mass units lower than the molecular ion, indicating that the complexes probably had lost a $Fe(CO)_4$ fragment. This means that under the conditions used, the conversion of **4** to **3** takes place. When using low ionization temperatures all complexes showed a signal belonging to **4** but this signal always remained very weak.

NMR spectroscopy

The ^{1}H NMR and ^{13}C NMR data are listed in Tables 9 and 10, respectively. In the NMR spectra of non-coordinated R-Pyca ligands, the imine proton and imine carbon atoms absorb in the 8–9 and 155–165 ppm regions, respectively [6], where also the imine protons and the imine carbons of the σ-N,σ-N′ coordinated α-diimine ligands are found [1]. This is also observed for complexes **4a–c** for which the imine proton and imine carbon resonances vary from 8.55 to 8.66 and 160 to 166 ppm, respectively. These values are comparable to the values observed for the isostructural $Os_3(CO)_{10}$(R-Pyca) complexes in which the imine proton and imine carbon chemical shifts lie between 8 and 9 and 156 and 160 ppm [45], respectively.

However, if an α-diimine ligand uses the π-electrons of a C=N moiety for coordination the resonances of the imine proton and the imine carbon atom of the η^2-bonded imine moiety are shifted drastically to higher field owing to the π-backbonding of the metal [1, 6], resulting in chemical shifts varying from 3.78 to 3.80 ppm and from 61 to 67 ppm for complexes **3a–c**.

Fluxional behaviour of complexes 4

The ^{13}CO resonances of complexes **4** presented in Table 10 were observed at 190 K. At higher temperatures the CO ligands are involved in fluxional movements which will first be discussed for $Fe_2Ru(CO)_{10}$(^{t}Bu-Pyca) (**4c**). A selection of the spectra obtained at different temperatures is shown in Fig. 4 and the assignment of the signals is shown in Figs. 4 and 5.

TABLE 8. Mass spectroscopic and IR data and elemental analyses of the complexes **3a–c** and **4a–c**

Complex	FD-mass obs. (calc.)	IR (cm^{-1}) ν(C=O)	Elemental analysis: obs. (calc.) (%)		
			C	H	N
3a[a]	474 (473.19)	2071(s), 2009(vs), 2005(sh), 1989(s), 1942(sh), 1938(s)	38.05 (38.07)	2.62 (2.56)	5.83 (5.92)
3b[a]	514 (513.25)	2068(s), 2006(vs), 1988(s), 1939(sh), 1936(s)	42.12 (42.12)	3.12 (3.14)	5.50 (5.46)
3c[a]	488 (487.21)	2070(s), 2006(vs), 2003(sh), 1988(vs), 1937(vs)	39.40 (39.44)	2.91 (2.90)	5.54 (5.75)
4a[b]	642 (641.08)	2062(s), 2015(vs), 2010(vs), 1982(s, br), 1952(sh), 1764(m)	35.37 (35.60)	1.86 (1.89)	4.14 (4.37)
4b[b]	514 (681.16)	2061(s), 2012(vs), 1986(s, br) 1955(sh), 1766(m)	38.68 (38.79)	2.44 (2.37)	4.19 (4.11)
4c[b]	488 (655.10)	2060(s), 2016(vs), 1997(vs), 1980(sh), 1960(sh), 1782(m)	36.62 (36.67)	2.17 (2.15)	4.14 (4.28)

[a]Hexane solution. [b]CH_2Cl_2 solution.

TABLE 9. ^{1}H NMR data of the complexes **3a–c** and **4a–c**

3a[a]	7.90 (1H, d, 5 Hz, py-H6); 7.35 (1H, dd, 7 Hz/7.5 Hz, py-H4); 7.09 (1H, d, 7.5 Hz, py-H3); 6.64 (1H, dd, 5 Hz/7.5 Hz, py-H5); 3.78 (1H, s, N=CH); 3.27 (1H, sept, 6.5 Hz, ^{i}Pr-CH); 1.47/1.38 (3H/3H, d, 6.5 Hz, ^{i}Pr-Me)
3b[a]	7.89 (1H, d, 5 Hz, py-H6); 7.35 (1H, dd, 7 Hz/8 Hz, py-H4); 7.09 (1H, d, 8 Hz, py-H3); 6.64 (1H, dd, 5 Hz/7 Hz, py-H5); 3.80 (1H, s, N=CH); 2.73 (1H, m, ^{c}Hex-CH); 2.1–1.2 (10H, m, ^{c}Hex-CH_2)
3c[a]	7.93 (1H, d, 5 Hz, py-H6); 7.40 (1H, dd, 7 Hz/8 Hz, py-H4); 7.11 (1H, d, 8 Hz, py-H3); 6.69 (1H, dd, 5 Hz/7 Hz, py-H5); 3.80 (1H, s, N=CH); 1.37 (9H, s, ^{t}Bu-CH_3)
4a[a]	9.83 (1H, d, 5 Hz, py-H6); 8.62 (1H, s, N=CH); 8.13–7.80 (3H, m, py-H3/H4/H5); 5.16 (1H, sept, 6.5 Hz, ^{i}Pr-CH); 1.57 (6H, d, 6.5 Hz, ^{i}Pr−Me)
4b[b]	9.85 (1H, d, 5 Hz, py-H6); 8.55 (1H, s, N=CH); 8.07 (1H, dd, 6 Hz/7.5 Hz, py-H4); 7.87 (1H, d, 7.5 Hz, py-H3); 7.76 (1H, dd, 6 Hz/5 Hz, py-H5); 2.21(1H, m, ^{c}Hex-CH); 1.75–1.50 (10H, m, ^{c}Hex-CH_2)
4c[a]	9.39 (1H, d, 5 Hz, py-H6); 8.66 (1H, s, N=CH); 8.16–8.08 (1H, m, py-H3/H4); 7.67 (1H, dd, 8 Hz/5 Hz, py-H5); 1.44 (9H, s, ^{t}Bu-CH_3)

[a]$CDCl_3$, 100 MHz, 293 K. [b]$CDCl_3$, 300 MHz, 293 K.

TABLE 10. ^{13}C NMR data of the complexes **3a–c** and **4a–c**

3a[a]	27.4/28.6 (^{i}Pr-CH_3); 66.8 (N=CH); 67.3 (^{i}Pr-CH); 118.1 (py-C^5); 119.4 (py-C^3); 138.2 (py-C^4); 151.0 (py-C^6); 173.2 (py-C^2); 186.5/197.8/204.6 (Ru–CO); 216.3 (Fe–CO)
3b[a]	26.0/26.3/27.0/37.9/40.3 (^{c}Hex-CH_2); 66.1 (N=CH); 74.5 (^{c}Hex-CH); 117.5 (py-C^5); 118.7 (py-C^3); 137.6 (py-C^4); 151.4 (py-C^6); 172.4 (py-C^2); 185.7/197.2/204.0 (Ru–CO); 215.8 (Fe–CO)
3c[a]	33.2 (^{t}Bu-CH_3); 61.2 (N=CH); 63.1 (^{t}Bu-CCH_3); 117.8 (py-C^5); 119.0 (py-C^3); 137.7 (py-C^4); 151.2 (py-C^6); 172.9 (py-C^2); 186.1/197.2/204.3 (Ru–CO); 216.2 (Fe–CO)
4a[b]	16.4/18.6 (^{i}Pr-CH_3); 54.8 (^{i}Pr-CH); 126.0 (py-C^5); 127.8 (py-C^3); 138.3 (py-C^4); 146.8 (py-C^6); 152.2 (py-C^2); 161.1 (N=CH); 181.5 (CO); 206.0 (2×CO); 209.3 (CO); 212.0 (CO); 214.6 (CO); 218.0 (CO); 219.1 (CO); 237.1 (CO); 251.8 (CO)
4a[c,d]	22.2/26[e] (^{i}Pr-CH_3); 58.6 (^{i}Pr-CH); 126.9 (py-C^5); 129.7 (py-C^3); 141.9 (py-C^4); 150.6 (py-C^6); 156.1 (py-C^2); 164.9 (N=CH); 185.3 (CO_a); 208.2 (CO_c); 209.8 (CO); 213.3 (CO), 215.5 (CO_d); 218.1 (CO_e); 221.7 (CO); 222.8 (CO); 240.0 (CO_b); 255.1 (CO_b)
4b[b]	23.3/23.4/23.8/29.3/34.4 (^{c}Hex-CH_2); 62.4 (^{c}Hex-CH); 126.0 (py-C^5); 127.7 (py-C^3); 138.2 (py-C^4); 146.6 (py-C^6); 152.1 (py-C^2); 161.3 (N=CH); 181.2 (CO); 206.0 (2×CO); 209.1 (CO); 212.0 (CO); 214.1 (CO); 218.0 (CO); 218.6 (CO); 239.1 (CO); 252.0 (CO)
4c[b,f]	27[e] (^{t}Bu-CH_3); 64.5 (^{t}Bu-CCH_3); 125.3 (py-C^5); 128.7 (py-C^3); 138.6 (py-C^4); 152.0 (py-C^6); 154.5 (py-C^2); 162.7 (N=CH); 191.0 (CO_a); 201.5 (CO_c); 210.5 (CO_c); 210.7 (CO_e); 213.6 (CO_c); 215.3 (CO_e); 237.3 (CO_b); 247.4 (CO_b)
4c[d]	31.3 (^{t}Bu-CH_3); 68[e] (^{t}Bu-CCH_3); 129.1 (py-C^5); 132.4 (py-C^3); 142.3 (py-C^4); 156.3 (py-C^6); 158.5 (py-C^2); 166.4 (N=CH); 194.9 (CO_a); 205.8 (CO_c); 208.9 (CO_d); 209.3 (CO_d); 214.7 (CO_c); 214.8 (CO_e); 218.3 (CO_c); 219.5 (CO_e); 239.4 (CO_b); 250.0 (CO_b)

[a]$CDCl_3$, 25 MHz, 263 K. [b]Acetone-d_6, 75 MHz, 190 K. [c]Assignment of carbonyls according to Fig. 7. [d]THF-d_8, 75 MHz, 190 K. [e]Exact position not obtained due to signals belonging to the solvent. [f]Two carbonyls (CO_d) probably under solvent signal.

The assignments of the terminal carbonyl (a) at the Ru centre and the two bridging carbonyls (b_1) and (b_2) are based on their chemical shifts. The assignment of the carbonyls (c) coordinated to Fe(1) is derived from their observed fluxional behaviour (*vide infra*), while that of the carbonyls (d) and (e) coordinated to Fe(2) are based on the observed fluxional behaviour and on the observation that axial carbonyl ligands generally resonate at lower field than equatorial carbonyl ligands [38, 46].

At about 185 K a broadening of the signals at 218.3, 214.7 and 205.8 ppm occurs, while at about 208 K the signals at 250.0, 239.4, 219.5 and 214.8 ppm start to broaden, and finally the signals at 209.3, 208.9 and 194.9 ppm broaden at about 228 K. Between 253 and 298 K all signals have disappeared in the baseline, while a broad signal becomes visible at 217.1 ppm at 323 K, which is close to the average value (217.56).

The rearrangements occurring in the various temperature ranges clearly overlap, making it impossible

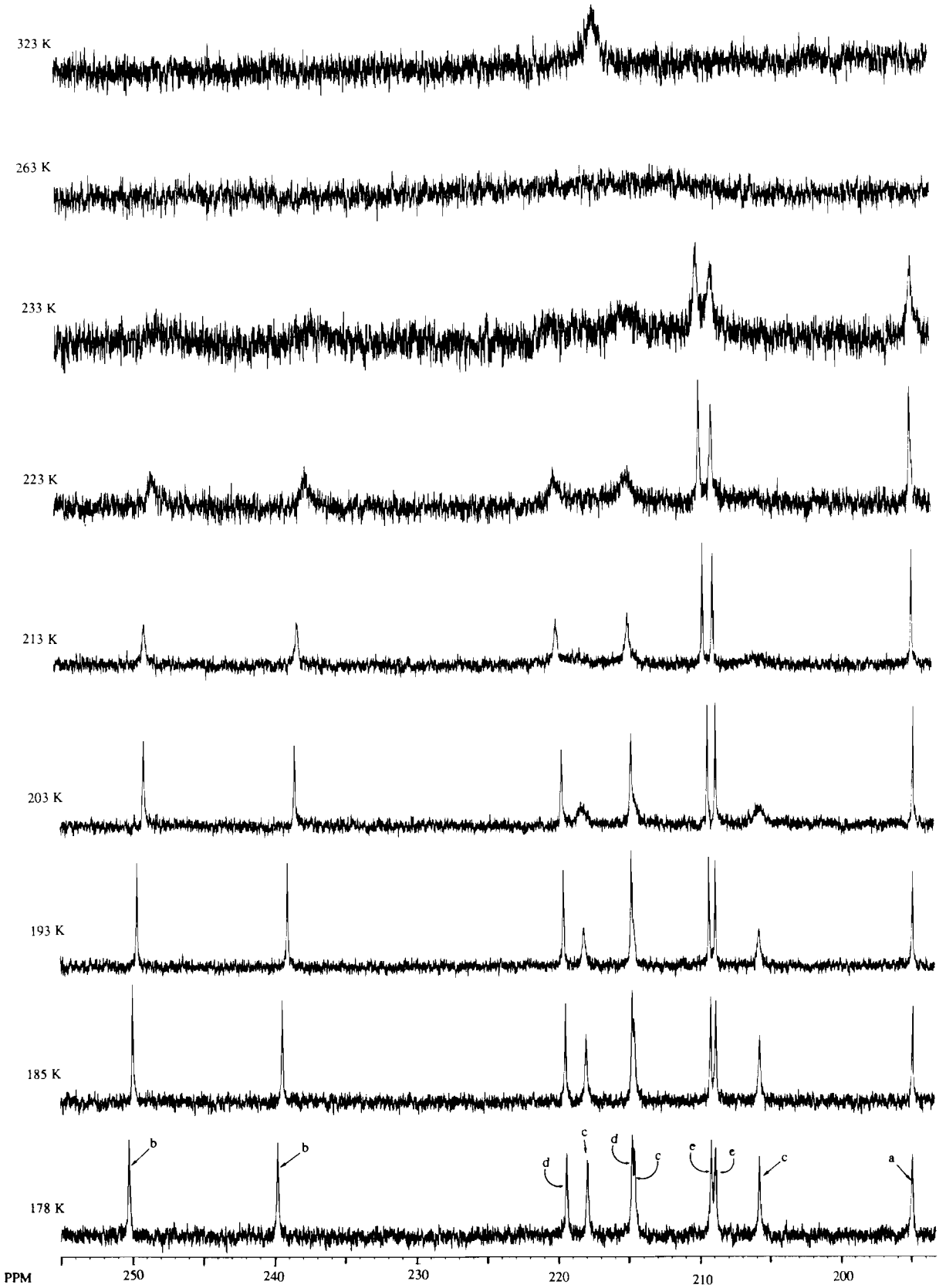

Fig. 4. Variable temperature ^{13}C NMR of $Fe_2Ru(CO)_{10}(^tBu\text{-}Pyca)$ (**4c**).

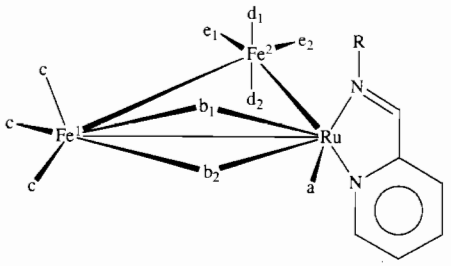

Fig. 5. Assignment of the carbonyl ligands in complexes **4**.

to observe the stepwise coalescence of each set of signals separately. Due to the chemical conversion of the complexes **4** to **3** at higher temperatures we have not been able to reach the fast exchange limit, although, as shown in Fig. 4, this situation has almost been obtained.

Several types of fluxional processes have been proposed [46–51] to explain the temperature dependent NMR spectra of trinuclear carbonyl clusters. In our case clearly several processes take place as well, as can be seen from the different temperatures at which the broadening of the various signals starts.

The lowest temperature process (from 178 to 208 K) may be explained by a scrambling of only the carbonyls coordinated to Fe(1) [51]. At a temperature of about 208 K the axial carbonyls of Fe(2) (d_1, d_2) and the two bridging carbonyls (b_1, b_2) start to become involved in the fluxional behaviour as well. The suggested mechanism (Fig. 6) is consistent with the one proposed by Cotton *et al.* [47], which involves the interchange above the plane of the metal triangle of the carbonyl ligands (b_1) and (d_1) together with one of the carbonyls (c) coordinated to Fe(1), whereas (b_2) and (d_2) exchange below the metal triangle together with also a carbonyl (c) coordinated to Fe(1).

Due to the inherent asymmetric character of the ^{t}Bu-Pyca ligand one would expect a difference in energy barriers for the exchange processes above the metal triangle (i.e. b_1, c, d_1; Figs. 5 and 6) and below the metal triangle (i.e. b_2, c, d_2; Figs. 5 and 6), respectively. However, this is not observed for **4c**, as can be concluded from the observation that the signals of all carbonyls above and below the metal triangle broaden in the same temperature range.

At about 228 K the carbonyl coordinated to Ru in an equatorial position (a) also becomes involved in the fluxional behaviour, while the carbonyls equatorially coordinated to Fe_2 (i.e. e_1 and e_2) broaden in the same temperature range. The participation of these carbonyls may be rationalized by a process as outlined in Fig. 7. This process may be considered as a rotation of the equatorial carbonyls (a), (c), (e_1) and (e_2) within the plane of the metal triangle. During this process the Pyca ligand is forced to move from a position in line with the Fe_1–Ru axis to a position in line with the Fe_2–Ru axis. This process therefore rationalizes at the same time why the diastereotopic ^{i}Pr-Me groups in the case of **4a** (*vide infra*) become equivalent in this temperature range.

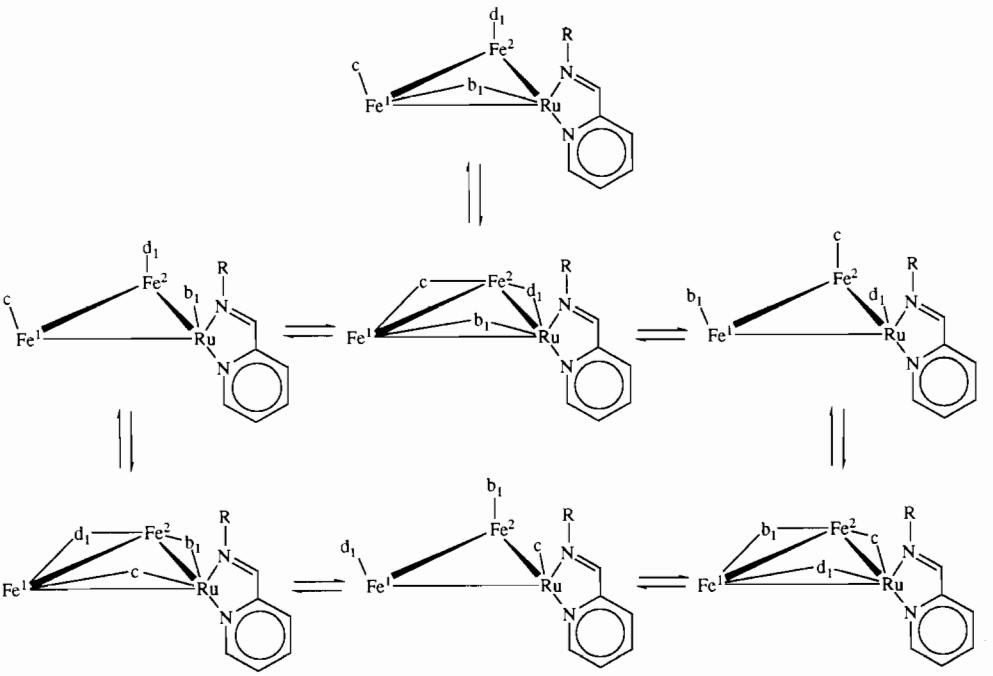

Fig. 6. Proposed exchange process for carbonyls (b), (c) and (d) of the complexes $Fe_2Ru(CO)_{10}$(R-Pyca) (**4c**) above and below the metal triangle. (Only the process above the metal triangle has been outlined in the Fig.)

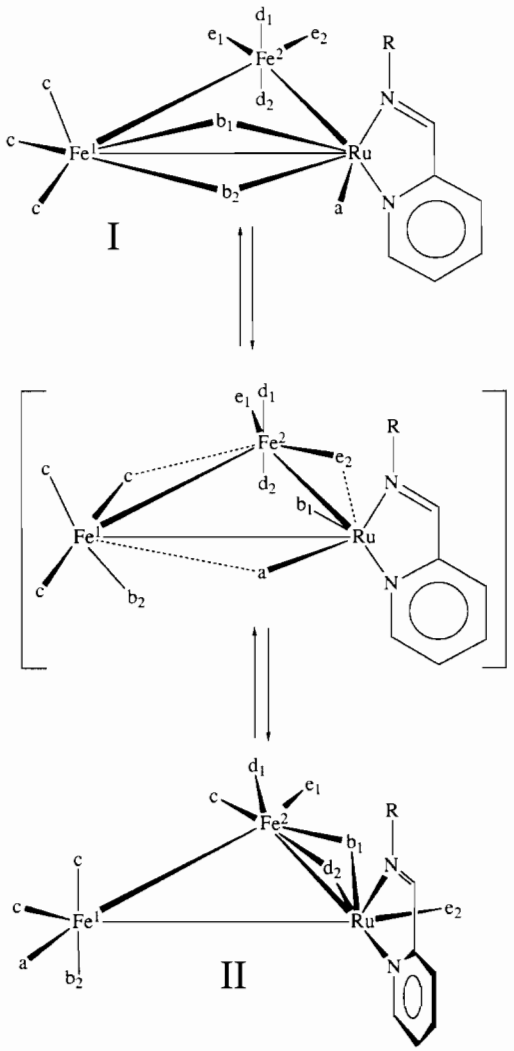

Fig. 7. Proposed fluxional process for complex **4c** involving exchange of carbonyls (e_1), (e_2) and (a).

A possible explanation for the participation of carbonyl (a) to the complete carbonyl scrambling at higher temperatures is a terminal/bridge exchange perpendicular to the metal triangle as shown in Fig. 8. Via this process, which has already been proposed by Cotton *et al.* [47], the carbonyls (a), (b_1), (b_2) and (c) are able to scramble within a plane perpendicular to the metal triangle.

It should be emphasized that additional mechanisms may explain a scrambling of all carbonyl ligands in the fast exchange limit. Processes like a rocking motion of the α-diimine ligand [38, 48], rotation of the α-diimine after a temporary rupture of one of the Ru–N bonds, merry-go-round scrambling processes of the carbonyl ligands [49] or hidden processes as described by Cotton *et al.* [47] may very well occur as well in our case, and it is not possible to tell which processes do occur in the fast exchange limit and which do not.

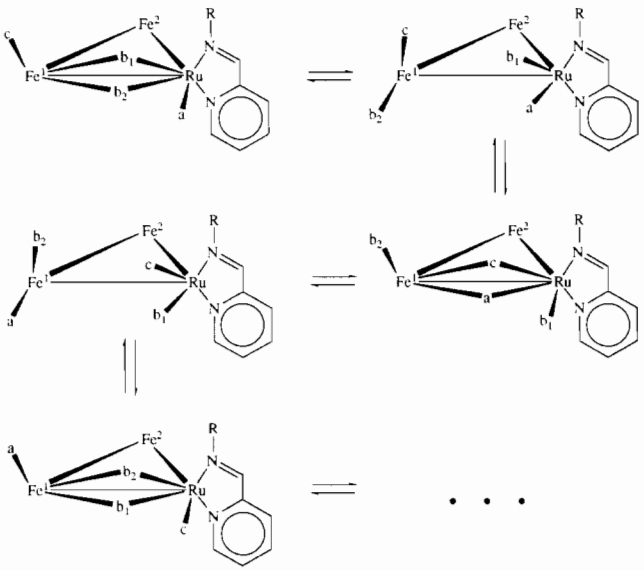

Fig. 8. Possible explanation for the participation of carbonyl (a) to the total scrambling of all carbonyl ligands in the fast exchange limit.

Comparison of the results for $Fe_2Ru(CO)_{10}$(^{i}Pr-Pyca) (**4a**) with those for **4c** shows some interesting differences. The lowest temperature process for **4a** involves a broadening of the signals at 255.1, 215.5 and 208.3 ppm, starting at about 185 K and resulting in a disappearance of these signals in the baseline at about 203 K. At a temperature of about 213 K all other carbonyl ligands start to broaden, indicating that the various processes occurring for **4a** overlap to a stronger degree than in the case of **4c**. At a temperature of 243 K all carbonyl signals have disappeared in the baseline.

The lowest temperature process in this case may be rationalized by the exchange of only the carbonyls (b_1), (c) and (d_1) above the metal triangle as shown in Fig. 6*. Probably the replacement of the ^{t}Bu-group by the sterically less demanding ^{i}Pr-group explains for **4a** the occurrence of this process above the metal triangle at a much lower temperature as compared to **4c**. It is interesting to note that it is rather unique that we are able to observe separately the exchange processes above and below the trimetallic array, especially at such low temperatures (<200 K). Even in the case of $Ru_3(CO)_{10}$(1,2-diazine) [47], where one of the sides of the metal triangle is completely free of steric interactions of the diazine ligand, such an exchange did not take place at temperatures below −30 °C.

*From the chemical shifts it becomes obvious that, in contrast to **4c**, in the case of **4a** a bridging carbonyl is involved in the lowest temperature process, clearly indicating that we are dealing with a different process. Their seems no obvious explanation for the fact that the lowest temperature process in the case of **4c**, i.e. a scrambling of the three carbonyl ligands coordinated to Fe(1), in the case of **4a** needs higher temperatures to occur as compared to the case of **4c**.

The ^1H NMR spectrum of **4a** shows separate signals for the two diastereotopic ^{i}Pr-Me groups at a temperature of 178 K. Upon raising the temperature these signals start to broaden at about 208 K and appear as one doublet at 238 K. The respective ^{13}C NMR resonances of the two methyl group broaden and coalesce in the same temperature range and reappear as one signal at a temperature of about 253 K. Since the two ^{i}Pr-Me groups of the ^{i}Pr-Pyca ligand occupy different positions above the metal triangle this may be rationalized by a movement of the Pyca ligand from a position along the Fe(1)–Ru axis to a position along the Fe(2)–Ru axis (Fig. 7).

Finally, it should be noted that the α-diimine ligand in complexes **4a**/**4c** has a greatly retarding effect on the fluxional movements, since the ^{13}C NMR signals of the carbonyl groups of the parent compound $Fe_2Ru(CO)_{12}$ are already in the fast exchange limit at 243 K [51]. It is understandable that especially the participation of the equatorial carbonyls (a and e) in the exchange process is greatly hindered by the presence of the α-diimine ligand.

Formation of complexes 3 and 4

The reaction of $Ru_2(CO)_4(R\text{-}Pyca)_2$ (**1a–c**) with $Fe_2(CO)_9$ (Scheme 1) leads to the formation of the new heteronuclear complexes $FeRu(CO)_6(R\text{-}Pyca)$ (**3a–c**) and $Fe_2Ru(CO)_{10}(R\text{-}Pyca)$ (**4c–c**), thus giving access to the only unknown member of the series of complexes $M_2(CO)_6(L)$ ($M_2 = Fe_2$, FeRu, Ru_2; L = R-DAB, R-Pyca). The product distribution depends both on the reaction temperature and on the solvent. When the reaction was performed in toluene (or benzene) at 80 °C complex **3** was the only product obtained in 75–80% yield. At room temperature the ratio of **3**/**4** varied from 1.1 in toluene (or benzene) via 0.65 in Et_2O to 0.1 in THF. Attempts to perform the reaction in acetonitrile failed due to insolubility of **1** and probably also due to the fact that the $Fe(CO)_4(MeCN)$ formed is too resistant to substitution*. The combined yield of **3** and **4** varied in all cases from 75 to 85% (based on the $Ru_2(CO)_4(R\text{-}Pyca)_2$ (**1**) consumed).

It should be mentioned that in the reaction of **1** with $Fe_2(CO)_9$ the substitution is not very effective, since a very large excess of $Fe_2(CO)_9$ is needed, with the unfortunate consequence that large amounts of $Fe(CO)_5$ and $Fe_3(CO)_{12}$ are formed as side products**. As expected from the strong temperature dependence of the product distribution it was observed that the thermal stability of **4** is low, since upon heating conversion to **3** has been observed.

Complex **1** reacted with $Ru_3(CO)_{12}$ at elevated temperatures to yield $Ru_2(CO)_6(R\text{-}Pyca)$ [6]. As $Ru_3(CO)_{12}$ needs much higher temperatures to form $M(CO)_4$ fragments than $Fe_2(CO)_9$, the reaction conditions used in reacting **1** with $Ru(CO)_4$ fragments were obviously too severe to isolate a homotrinuclear analogon of **4**. Attempts to use $Ru(CO)_5$ as a source for $Ru(CO)_4$ fragments failed because the preparation of $Ru(CO)_5$ only proceeds well in alkane solution [53]. As **1** hardly dissolves in alkanes, and since the non-coordinating alkanes are not sufficiently able to stabilize the unsaturated $Ru(CO)_4$ species, the short lived $Ru(CO)_4$ fragments formed did not react with **1** but recombined to form $Ru_3(CO)_{12}$.

The reaction is also applicable for the synthesis of $FeRu(CO)_6(R\text{-}DAB)$ [3] using $Ru_2(CO)_4(R\text{-}DAB)_2$ [4] and $Fe_2(CO)_9$. This reaction needs higher temperatures and longer reaction times than the reaction of **1** with $Fe_2(CO)_9$ which is probably caused by the better π-accepting ability of the DAB ligand when compared to R-Pyca [1]. This leads to a stronger metal–η^2-C=N bond for the DAB ligand, thus making it more difficult to substitute this imine moiety.

Since besides $FeRu(CO)_6(R\text{-}Pyca)$ (**3**) the complexes $Ru_2(CO)_6(R\text{-}Pyca)$ and $FeRu(CO)_6(R\text{-}DAB)$ can also be prepared in this way, reaction of $Ru_2(CO)_4(L)_2$ (L = R-DAB, R-Pyca) with $M(CO)_4$ fragments may be used as a general route for the preparation of complexes $M_2(CO)_6(\alpha\text{-diimine})$. However, for the preparation of $MRu(CO)_6(L)$ complexes other than **3** other synthetic routes are preferable [3–5, 6].

Scheme 2 shows a proposed mechanism for the reaction of **1** with $Fe_2(CO)_9$, based on substitution of the η^2-coordinated imine bond by the unsaturated species $Fe(CO)_4$. In the first step of the reaction sequence one of the η^2-bonded imine moieties is substituted [3, 54–56] by a $Fe(CO)_4$ fragment which is easily formed from $Fe_2(CO)_9$, leading to the unsaturated intermediate **XI**. This intermediate can either react back to the starting compound or react with a second $Fe(CO)_4$ fragment, thus producing two molecules of intermediate **X2**, which react further to either **3** or **4**. Which course is chosen depends on the concentration of the $Fe(CO)_4$ species. One would therefore expect, as is indeed the case (*vide supra*), a solvent dependence of the reaction, since stronger coordinating solvents are better able to stabilize $Fe(CO)_4$ fragments and therefore enhance the formation of **4** with respect to **3**.

An indication for the suggestion that $Fe(CO)_4$ fragments are involved in the reaction and not the starting compound $Fe_2(CO)_9$ may be deduced from the reaction

*The comparable $Fe(CO)_4$(pyridine) was also reported to be quite stable [52].

$Fe(CO)_5$ is formed as a side product from $Fe_2(CO)_9$ via $Fe_2(CO)_9 \rightarrow Fe(CO)_5 + Fe(CO)_4$. The $Fe(CO)_4$ fragments that do not react with **1 trimerize forming $Fe_3(CO)_{12}$. For more information about this behaviour see ref. 16.

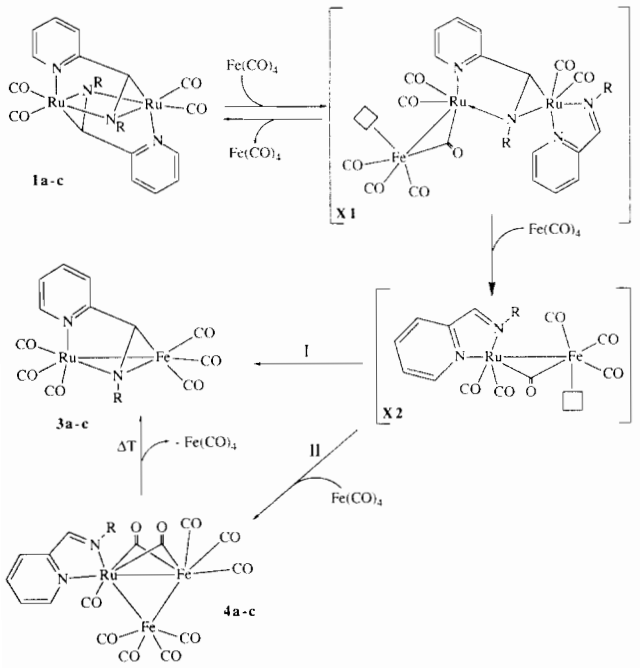

Scheme 2. Proposed mechanism for the reaction $Ru_2(CO)_4(R\text{-}Pyca)_2$ (**1a–c**) and $Fe_2(CO)_9$ (**2**).

of $Ru(CO)_3(^iPr\text{-}DAB)$ with $H_2Fe(CO)_4$ from which $Fe_2Ru(CO)_{10}(^iPr\text{-}DAB)$ is formed as a side product [11].

Supplementary material

Tables of the fractional coordinates, bond lengths and bond angles of all H atoms of **3a** (3 pages) and **4a** (3 pages), and listings of structure factor amplitudes for **3a** (13 pages) and **4a** (18 pages) can be obtained from the authors on request.

Acknowledgements

The authors thank Dr H.-W. Frühauf for helpful suggestions both during the experimental work and during the preparation of the manuscript. We thank D. Heijdenrijk for collecting the X-ray data.

References

1 (a) G. van Koten and K. Vrieze, *Adv. Organomet. Chem., 21* (1982) 151; (b) K. Vrieze, *J. Organomet. Chem., 300* (1986) 307; (c) G. van Koten and K. Vrieze, *Recl. Trav. Chim. Pays-Bas, 100* (1981) 129; (d) K. Vrieze and G. van Koten, *Inorg. Chim. Acta, 100* (1985) 79.

2 (a) J. Keijsper, L. H. Polm, G. van Koten, K. Vrieze, E. Nielsen and C. H. Stam, *Organometallics, 4* (1985) 2006; (b) J. Keijsper, L. H. Polm, G. van Koten, K. Vrieze, K. Goubitz and C. H. Stam, *Organometallics, 4* (1985) 1876; (c) L. H. Staal, G. van Koten, K. Vrieze, B. van Santen and C. H. Stam, *Inorg. Chem., 20* (1981) 3598; (d) J. Keijsper, L. H. Polm, G. van Koten, K. Vrieze, C. H. Stam and J.-D. Schagen, *Inorg. Chim. Acta, 103* (1985) 137; (e) L. H. Polm, G. van Koten, K. Vrieze, C. H. Stam and W. C. J. van Tunen, *J. Chem. Soc., Chem. Commun.,* (1983) 1177; (f) H.-W. Frühauf and F. Seils, *J. Organomet. Chem., 323* (1987) 67.

3 R. Zoet, K. Goubitz, C. J. G. van Halen, F. Muller, M. van Wijnkoop, C. H. Stam, G. van Koten and K. Vrieze, *Inorg. Chim. Acta, 149* (1988) 193.

4 L. H. Staal, L. H. Polm, R. W. Balk, G. van Koten, K. Vrieze and A. M. F. Brouwers, *Inorg. Chem., 19* (1980) 3343.

5 H.-W. Frühauf, A. Landers, R. Goddard and C. Krüger, *Angew. Chem., 90* (1978) 56.

6 L. H. Polm, G. van Koten, C. J. Elsevier, K. Vrieze, B. F. K. van Santen and C. H. Stam, *J. Organomet. Chem., 304* (1986) 353.

7 R. Zoet, C. A. A. Duineveld, C. J. Elsevier, K. Goubitz, D. Heijdenrijk, G. van Koten, C. H. Stam, P. Versloot, K. Vrieze and M. van Wijnkoop, *Organometallics, 8* (1989) 23.

8 (a) F. Muller and K. Vrieze, in J. J. Ziolkowski (ed.), *Coordination Chemistry and Catalysis,* World Scientific, Singapore, 1988; (b) C. J. Elsevier, F. Muller, K. Vrieze and R. Zoet, *New J. Chem., 12* (1988) 571.

9 F. Muller, K. A. A. Duineveld, D. Heijdenrijk, G. van Koten, M. J. A. Kraakman, C. H. Stam, K. Vrieze, R. Zoet and M. C. Zoutberg, *Organometallics, 8* (1989) 982.

10 F. Muller, D. Heijdenrijk, G. van Koten, M. J. A. Kraakman, K. Vrieze and M. C. Zoutberg, *Organometallics, 8* (1989) 1331.

11 M. J. A. Kraakman, K. Goubitz, M. Numan and K. Vrieze, *Inorg. Chim. Acta, 202* (1992) 197.

12 M. J. A. Kraakman, T. C. de Koning, P. P. M. de Lange, K. Vrieze, H. Kooijman and A. L. Spek, *Inorg. Chim. Acta, 203* (1992) 145.

13 L. H. Staal, G. van Koten, R. H. Fokkens and N. M. M. Nibbering, *Inorg. Chim. Acta, 50* (1981) 205.

14 L. H. Polm, R. R. Andrea, C. J. Elsevier, J. M. Ernsting, G. van Koten, C. H. Stam, D. J. Stufkens and K. Vrieze, *Organometallics, 6* (1987) 1096.

15 E. H. Braye and W. Hübel, *Inorg. Synth., 8* (1966) 178.

16 (a) D. F. Shriver and K. H. Whitmire, in G. Wilkinson, F. G. A. Stone and E. W. Abel (eds.), *Comprehensive Organometallic Chemistry,* Vol. IV, Pergamon, Oxford, 1982, pp. 255–258; (b) see also ref. 15 and 52.

17 (a) R. B. King, *Organometallic Synthesis,* Vol. 1, Academic Press, New York, 1965, p. 94; (b) R. B. King and F. G. A. Stone, *Inorg. Synth., 7* (1965) 193; (c) W. P. Fehlhammer, W. A. Herrmann and K. Öfele, in *Handbuch der Präparativen Anorganischen Chemie,* Ferdinand Enke, Stuttgart, 3rd edn., 1981, pp. 1827–1829.

18 H. Schenk and C. T. Kiers, *Simpel 83,* a program system for direct methods, in G. M. Sheldrick, C. Kruger and R. Goddard (eds.), *Crystallographic Computing 3,* Clarendon, Oxford, 1985.

19 N. Walker and D. Stuart, *Acta Crystallogr., Sect. A, 39* (1983) 158.

20 D. T. Cromer and J. B. Mann, *Acta Crystallogr., Sect. A, 24* (1968) 321.

21 D. T. Cromer and J. B. Mann, *International Tables for X-ray Crystallography,* Vol. IV, Kynoch, Birmingham, UK, 1974, p. 55.

22 J. M. Stewart, P. A. Machin, C. W. Dickinson, H. L. Ammon, H. Heck and H. Flack, The X-ray system, *Tech. Rep. TR-446,* Computer Science Centre, University of Maryland, College Park, MD, 1976.

23 W. D. S. Motherwell and W. Clegg, *PLUTO,* program for plotting molecular and crystal structures, University of Cambridge, UK, 1978.

24 T. Venäläinen and T. Pakkanen, *J. Organomet. Chem., 266* (1984) 269.

25 D. A. Roberts and G. L. Geoffroy, in G. Wilkinson, F. G. A. Stone and E. W. Abel (eds.), *Comprehensive Organometallic Chemistry,* Pergamon, Oxford, 1982, Ch. 40.

26 J. Keijsper, G. van Koten, H. van der Poel, L. H. Polm, P. F. A. B. Seignette, R. Varenhorst, C. H. Stam and K. Vrieze, *Polyhedron, 2* (1983) 1111.

27 L. H. Staal, J. Keijsper, G. van Koten, K. Vrieze, J. A. Cras and W. P. Bosman, *Inorg. Chem., 20* (1981) 555.

28 R. Zoet and K. Vrieze, unpublished results.

29 M. J. A. Kraakman, H. Kooijman, A. L. Spek and K. Vrieze, *Organometallics,* in press.

30 (a) F. A. Cotton, *Prog. Inorg. Chem., 21* (1976) 1; (b) R. Colton and M. J. McCormick, *Coord. Chem. Rev., 31* (1980) 1.

31 T. Venäläinen, J. Pursiainen and T. Pakkanen, *J. Chem. Soc., Chem. Commun.,* (1985) 1348.

32 M. I. Bruce, M. G. Humphrey, M. R. Snow, E. R. T. Tiekink and R. C. Wallis, *J. Organomet. Chem., 314* (1986) 311.

33 (a) R. Mason and A. I. M. Rae, *J. Chem. Soc. A,* (1968) 778; (b) M. R. Churchill, F. J. Hollander and J. P. Hutchinson, *Inorg. Chem., 16* (1977) 2655.

34 M. I. Bruce, M. J. Liddell, O. Shawkataly bin, I. Bytheway, B. W. Skelton and A. H. White, *J. Organomet. Chem., 369* (1989) 217.

35 E. J. Forbes, N. Goodhand, D. L. Jones and T. A. Hamor, *J. Organomet. Chem., 182* (1979) 143.

36 D. G. Evans and D. M. P. Mingos, *J. Organomet. Chem., 232* (1982) 171.

37 R. Shojaie and J. D. Atwood, *Inorg. Chem., 26* (1987) 2199.

38 R. Zoet, D. Heijdenrijk, J. T. B. H. Jastrzebski, G. van Koten, T. Mahabiersing, C. H. Stam and K. Vrieze, *Organometallics, 7* (1988) 2108.

39 H. Adams, N. A. Bailey, N. A. Bentley and B. E. Mann, *J. Chem. Soc., Dalton Trans.,* (1989) 1831.

40 (a) M. I. Bruce, M. J. Liddell, C. A. Hughes, B. W. Skelton and A. H. White, *J. Organomet. Chem., 347* (1988) 157; (b) M. I. Bruce, M. J. Liddell, C. A. Hughes, J. M. Patrick, B. W. Skelton and A. H. White, *J. Organomet. Chem., 347* (1988) 181; (c) M. I. Bruce, M. J. Liddell, O. Shawkataly bin, C. A. Hughes, B. W. Skelton and A. H. White, *J. Organomet. Chem., 347* (1988) 207.

41 (a) C. J. Cardin, D. J. Cardin, N. B. Kelly, G. A. Lawless and M. B. Power, *J. Organomet. Chem., 341* (1988) 447; (b)P. A. Dawson, B. F. G. Johnson, J. Lewis, J. Puga, P. R. Raithby and M. J. Rosales, *J. Chem. Soc., Dalton Trans.,* (1982) 233.

42 (a) M. I. Bruce, G. N. Pain, C. A. Hughes, J. M. Patrick, B. W. Skelton and A. H. White, *J. Organomet. Chem., 307* (1986) 343; (b) M. I. Bruce, T. W. Hambley and B. K. Nicholson, *J. Chem. Soc., Dalton Trans.,* (1983) 2385; (c) M. I. Bruce, J. G. Matisons, R. C. Wallis, J. M. Patrick, B. W. Skelton and A. H. White, *J. Chem. Soc., Dalton Trans.,* (1983) 2365.

43 R. Y. Alex and R. K. Pomeroy, *J. Organomet. Chem., 284* (1985) 379.

44 (a) B. Ambwani, S. Chawla and A. Poë, *Inorg. Chem., 24* (1985) 2635; (b) D. A. Brandes and R. J. Puddephatt, *Inorg. Chim. Acta, 113* (1986) 17; (c) J. A. Clucas, D. F. Foster, M. M. Harding and A. K. Smith, *J. Chem. Soc., Dalton Trans.,* (1987) 277; (d) M. I. Bruce, T. W. Hambley, B. K. Nicholson and M. R. Snow, *J. Organomet. Chem., 235* (1982) 83; (e) J. A. Clucas, R. H. Dawson, P. A. Dolby, M. M. Harding, K. Pearson and A. K. Smith, *J. Organomet. Chem., 311* (1986) 153; (f) W. R. Cullen and D. A. Harbourne, *Inorg. Chem., 9* (1970) 1839; (g) S. Cartwright, J. A. Clucas, R. H. Dawson, D. F. Foster, M. M. Harding and A. K. Smith, *J. Organomet. Chem., 302* (1986) 403; (i) A. F. Dyke, J. E. Guerchais, S. A. R. Knox, J. Roué, R. L. Short, G. E. Taylor and P. Woodward, *J. Chem. Soc., Chem. Commun.,* (1981) 537.

45 R. Zoet, A. J. M. Duisenberg, G. van Koten, A. L. Spek and K. Vrieze, *Inorg. Chim. Acta, 148* (1988) 71.

46 S. Aime and L. Milone, *Prog. NMR Spectrosc., 11* (1977) 183.

47 F. A. Cotton, B. E. Hanson and J. D. Jamerson, *J. Am. Chem. Soc., 99* (1977) 6588.

48 E. G. Bryan, B. F. G. Johnson and J. Lewis, *J. Chem. Soc., Dalton Trans.,* (1977) 144.

49 A. J. Deeming, S. Donovan-Mtunzi, S. E. Kabir and P. J. Manning, *J. Chem. Soc., Dalton Trans.,* (1985) 1037.

50 (a) A. J. Deeming, S. Donovan-Mtunzi and S. E. Kabir, *J. Organomet. Chem., 276* (1984) C65; (b) H. Adams, N. A. Bailey, G. W. Bentley and B. E. Mann, *J. Chem. Soc., Dalton Trans.,* (1989) 1831.

51 A. Forster, B. F. G. Jonson, J. Lewis, T. W. Matheson, B. H. Robinson and W. G. Jackson, *J. Chem. Soc., Chem. Commun.,* (1974) 1042.

52 F. A. Cotton and J. M. Troup, *J. Am. Chem. Soc., 96* (1974) 3438.

53 (a) J. Malito, S. Markiewicz and A. Poë, *Inorg. Chem., 21* (1982) 4335; (b) M. F. Desrosiers, D. A. Wink, R. Trautman, A. E. Friedman and P. C. Ford, *J. Am. Chem. Soc., 108* (1986) 1917.

54 F. Muller, G. van Koten, K. Vrieze, K. A. A. Duineveld, D. Heijdenrijk, A. N. S. Mak and C. H. Stam, *Organometallics, 8* (1989) 1324.

55 W. P. Mul, C. J. Elsevier, H.-W. Frühauf, K. Vrieze, I. Pein, M. C. Zoutberg and C. H. Stam, *Inorg. Chem., 29* (1990) 2336.

56 (a) H.-W. Frühauf, F.-W. Grevels and A. Landers, *J. Organomet. Chem., 178* (1979) 349; (b) H.-W. Frühauf and G. Wolmershäuser, *Chem. Ber., 115* (1982) 1070.